

# A new silver ion conducting $\text{SbI}_3\text{--Ag}_4\text{P}_2\text{O}_7$ nanocomposite solid electrolyte

S. Austin Suthanthiraraj · R. Sarumathi

Received: 11 June 2012 / Accepted: 20 August 2012 / Published online: 19 September 2012  
© The Author(s) 2012. This article is published with open access at Springerlink.com

**Abstract** This paper presents an investigation on a new series of silver ion conducting nanocomposite materials of silver pyrophosphate-based solid electrolytes with various amounts of antimony iodide. The detailed electrical conductivity studies carried out by impedance spectroscopic analysis in the frequency range from 20 Hz to 1 MHz have shown that silver ionic conductivity attains a maximum value of  $4.1 \times 10^{-4} \text{ S cm}^{-1}$  at room temperature for the typical composition having 60 mol% of  $\text{SbI}_3$ . Powder samples characterized by X-ray diffraction, Fourier transform infrared spectroscopy, differential scanning calorimetric analysis and silver ionic transport studies were identified to indicate the existence of AgI, in addition to certain new phases in all the different compositions of the system. The conduction channel for  $\text{Ag}^+$  ions across phosphate network was found to get expanded by the presence of iodide ion. The formation of  $\text{P--O--M}$  ( $\text{M}=\text{Sb}^{3+}$ ) within the crystal structure is also favoured, where  $\text{Sb}^{3+}$  ions may serve as ionic cross-links between non-bridging oxygen of different phosphate groups. The field emission scanning electron microscopic investigations of their microstructures have suggested the presence of nanocomposites, leading to the observed electrical conductivity data coupled with many interesting features closely related to the particle size and practical application as solid electrolyte for the fabrication of solid-state battery at ambient conditions.

**Keywords** Silver pyrophosphate · FT-IR · Silver ion conductivity · FE-SEM

## Introduction

Solid electrolytes having high ionic conductivity and negligible electronic conductivity are called superion conducting or fast ion conducting (FIC) electrolytes. Nanophase solid electrolyte has attracted a great deal of attention in the past decade. The synthesis of ultra fine particles is one of the most important challenges today and such materials exhibit significantly improved characteristics when compared to their coarse grain counterparts (Dutta and Ghosh 2009). A number of FIC materials based on  $\text{Ag}^+$ ,  $\text{Li}^+$ ,  $\text{Cu}^+$ ,  $\text{Na}^+$  and  $\text{F}^-$  ions have already been reported (Padmasree et al. 2005) and those materials showing high conductivity due to  $\text{Ag}^+$  ion are mainly based on AgI. The ‘average structure like’  $\alpha$ -phase of silver iodide at room temperature has been stabilized by introducing stabilizing ions into the lattice, thus hindering the close packing of iodide ion, which may be the cause of low ionic conduction in  $\beta$ -phase of AgI (Takahashi 1973). The discovery of FIC materials and subsequent application of these materials in the fabrication of solid-state batteries have overcome a number of inherent disadvantages encountered with aqueous state cells. Among FIC materials of different kinds, pyrophosphate materials are more important because they can be easily prepared, possess simple composition, exhibit high ionic conductivity and have diverse applications (Anantharaj et al. 1986). Solid electrolytes with mobile  $\text{Ag}^+$  ions and higher conductivity at ambient conditions have had common oxy anions of elements with high charge radius ratio (e.g., B(III), Ge(IV), P(V), S(VI) and Mo(VI) etc.). (Sundar et al. 1987). In such systems, the glass-forming range is either narrow or is restricted to <60 % of the Ag halide. Silver ion conducting glasses are also interesting from an academic point of view and can be used as model systems for the development of

S. A. Suthanthiraraj (✉) · R. Sarumathi  
Department of Energy, University of Madras, Maraimalai  
Campus, Guindy, Chennai 600025, India  
e-mail: suthan98@gmail.com

solid-state batteries. Pyrophosphate itself is an interesting material from the point of view of ionic transport. Pyrophosphate groups dissociate into a variety of other polymeric anions of varying length when they are melted (Anantharaj et al. 1986). Because of this property, several solid electrolytes based on pyrophosphate can be prepared readily and ionic transport in these materials is mainly due to  $\text{Ag}^+$  ion. Thus, the potential of  $\text{Ag}_4\text{P}_2\text{O}_7$  as a FIC material suitable for  $\text{Ag}^+$  ion-based batteries is quite high. Silver phosphate materials doped with various monovalent metal halides have been prepared and it is concluded that the electrical conductivity has been enhanced on the addition of metal halides up to 15 wt % of concentration. In the case of divalent metal halide doping, the increase in conductivity was observed only up to 5 wt % (Das et al. 2010). Similarly, the conductivity of silver phosphate with the addition of iodides, di-iodides and tri-iodides has also been investigated (Takahashi et al. 2005). In view of this fact, an attempt has been made to study whether  $\text{Ag}_4\text{P}_2\text{O}_7$  can serve as a host for  $\text{SbI}_3$  instead of  $\text{AgI}$ , to synthesize a new solid electrolyte having high conductivity and better stability at ambient conditions.

## Experimental procedure

Powder specimens having various compositions of the solid electrolyte system  $(\text{Ag}_4\text{P}_2\text{O}_7)_{100-x} - (\text{SbI}_3)_x$ , ( $10 \leq x \leq 90$ ) were prepared by melt quenching technique. Silver pyrophosphate was prepared from commercially available analar grade silver nitrate and sodium pyrophosphate by double displacement reaction in solution and then dried at 393 K for 6 h (Anantharaj et al. 1986). The X-ray diffraction (XRD) pattern of silver pyrophosphate was compared with the literature data (JCPDS file no. 00-040-0058). Commercially available  $\text{SbI}_3$  and freshly prepared  $\text{Ag}_4\text{P}_2\text{O}_7$  were weighed according to their molecular weight percentage and mixed thoroughly. The powder mixture was then placed in a quartz tube and annealed at a temperature of 873 K for 24 h. The homogeneous melt obtained was then quenched in a liquid  $\text{N}_2$  bath and resulting solid materials were found to be thermodynamically stable under ambient storage conditions. During the course of the present investigation, all the powdered specimens of the chosen mixed system were pressed into circular pellets at a uniform pelletizing pressure of  $4,000 \text{ kg cm}^{-2}$  with a presumption that at this level of pressure the pellet density would be quite comparable to the bulk density of the sample under test. For this reason, no specific measurement pertaining to the density of materials was made. Furthermore, no heat treatment was also performed on these pellet specimens prior to analytical measurements owing to their stable nature. Powdered

specimens of individual compositions of the chosen system were made in the form of circular pellets of 8 mm diameter and 2.5 mm thick, under a constant pelletizing pressure of  $4,000 \text{ kg cm}^{-2}$  in conjunction with silver electrodes on either side. These electrodes comprised of metallic silver powder mixed with the appropriate sample in the weight ratio of 2:1 in order to minimize the effect of interfacial polarization during electrical conductivity measurements. Therefore, no conductive paste was applied for electrode contacts. Detailed electrical conductivity studies were carried out in the form of complex impedance analysis on such pellets, using a computer-controlled Hewlett-Packard model HP 4284A Precision LCR Meter, in the frequency range 20 Hz to 1 MHz and over the temperature range 298–423 K. Using the series of temperature-dependent complex impedance plots (i.e., plots of imaginary part,  $Z''$  against real part,  $Z'$  of impedance) obtained, the values of bulk resistance ( $R_b$ ) of these polycrystalline materials were estimated from the corresponding intercepts on the  $Z'$  axis (Boukamp 1986) and their dc electrical conductivity ( $\sigma$ ) values calculated using the relationship

$$\sigma = t/R_b A \quad (1)$$

where  $t$  is the thickness of the sample and  $A$  is the area of cross-section of the specimen. Knowing the value of bulk resistance  $R_b$ , and the dimension of the sample, the value of bulk electrical conductivity could be accurately estimated at each temperature for the different compositions. The room temperature ionic transport number of each sample was measured by employing both Wagner's polarization and emf techniques.

The ionic transport number ( $t_i$ ) data for various samples of the system were obtained by the Wagner's polarization method as follows: the solid sample made in the form of a pellet containing silver (non-blocking) and graphite (blocking) electrodes on either side was placed between two silver plates. A constant dc potential was applied to evaluate the current observed and potential difference across the sample simultaneously as a function of time. After 5–6 h, the current and voltage across the sample were found to attain steady-state values. If  $I_0$  and  $V_0$  are values of the initial current and initial voltage across the same pellet, respectively, and  $I_\infty$  and  $V_\infty$  are the respective values in the steady-state then

$$I_0/V_0 = G_t \quad (2)$$

and

$$I_\infty/V_\infty = G_e \quad (3)$$

where  $G_t$  and  $G_e$  denote the total conductance and electronic conductance of the sample pellet, respectively. From  $G_t$  and  $G_e$ , electronic transport number ( $t_e$ ) and ionic transport number ( $t_i$ ) were estimated using the relations

$$t_e = G_e/G_t \quad (4)$$

and

$$t_i = 1 - t_e \quad (5)$$

In order to find out the contribution of silver ions to the observed ionic conductivity in the various compositions, silver ionic transport number ( $t_{Ag^+}$ ) measurements were carried out on all the different compositions of the present system using the emf technique. Accordingly, electrochemical cells consisting of silver as anode, iodine as cathode and the sample under test as electrolyte were constructed and their open circuit voltages (OCVs) were measured at room temperature.

Morphology of the best conducting sample was analysed by means of scanning electron microscopy (SEM) using a HITACHI, S3400XN system. The microstructure of the sample was observed on a field emission scanning electron microscope (FESEM) HITACHI SU 6600 with single crystal 'W'.

Based on the electrical properties and structural aspects, the particular solid electrolyte having the maximum electrical conductivity (60 mol% of  $SbI_3$  in this work) was used in the fabrication of the solid-state cell. In the battery, silver metal acts as anode and the cathode material is a molar mixture of phenothiazine and iodine, in the molar ratio of 2:3, with a small amount of graphite. These materials were ground into fine powder, transferred into a die and pressed into a pellet at a pressure of  $5,000 \text{ kg cm}^{-2}$ . The electrolyte pellet was sandwiched between the cathode pellet and the silver metal anode inside the sample holder in order to construct the desired battery with the following configuration:

(–) Ag || silver and electrolyte || cathode (+)

For characterising the cell, its OCV and discharge characteristics were monitored at room temperature.

All the pure samples of  $Ag_4P_2O_7$  and  $SbI_3$  apart from freshly prepared powder specimens of the solid electrolyte system  $(Ag_4P_2O_7)_{100-x} - (SbI_3)_x$ , ( $10 \leq x \leq 90$ ) were analysed using a BRUKER D8 Advance model XRD system in order to identify and confirm the crystalline nature of various phases present within such compositions for  $2\theta$  values between  $20^\circ$  and  $80^\circ$  at room temperature.

Differential scanning calorimetric (DSC) measurements on all the synthesized samples were performed using a NETZSCH DSC 204 system, at the scanning rate of  $10 \text{ K min}^{-1}$ , in the temperature range of 303–773 K.

Room temperature Fourier transform infrared (FTIR) spectral studies were performed using a Perkin-Elmer RXI model spectrometer from  $4,000$  to  $400 \text{ cm}^{-1}$ .

## Results and discussion

Figure 1 depicts the observed complex impedance plots for the typical composition  $(Ag_4P_2O_7)_{40} - (SbI_3)_{60}$  at four different temperatures viz., 298, 303, 313 and 323 K, respectively. It is evident from Fig. 1 that each impedance plot exhibits a low frequency spike and a portion of semicircle at the high frequency side. The depressed semicircle at the high frequency region arises from the bulk relaxation and the low frequency spike arises from electrode/sample interfacial effects. Bulk resistance ( $R_b$ ) values were determined from the intercept on the real axis at the low frequency side. It is observed from these impedance plots that with the increase in temperature, the real axis intercept is shifted towards the origin, thus suggesting the fact that the bulk resistance value decreases and the electrical conductivity increases at elevated temperatures. The observed room temperature electrical conductivity ( $\sigma_{298 \text{ K}}$ ) data for pure  $Ag_4P_2O_7$ ,  $SbI_3$  and nine different compositions in the case of the present system  $(Ag_4P_2O_7)_{100-x} - (SbI_3)_x$ , ( $10 \leq x \leq 90$ ) along with corresponding values of ionic transport number data obtained from Wagner's technique and EMF are given in Table 1. This table shows that the conductivity increases with increasing dopant concentration up to a maximum of 60 mol%. The best conducting composition would correspond to the specimen having 60 mol%  $SbI_3$  possessing an electrical conductivity of  $4.1 \times 10^{-4} \text{ S cm}^{-1}$  at room temperature. The observed increasing trend in the case of electrical conductivity data may also be attributed as due to the structural phase transition occurring around 424 K as revealed by the present DSC data too (Murugesan et al. 2002). Figure 2 presents the variation of  $\log(\sigma T)$  as a function of inverse of absolute temperature for different compositions of the mixed system  $(Ag_4P_2O_7)_{100-x} - (SbI_3)_x$ , ( $10 \leq x \leq 90$ ). The observed

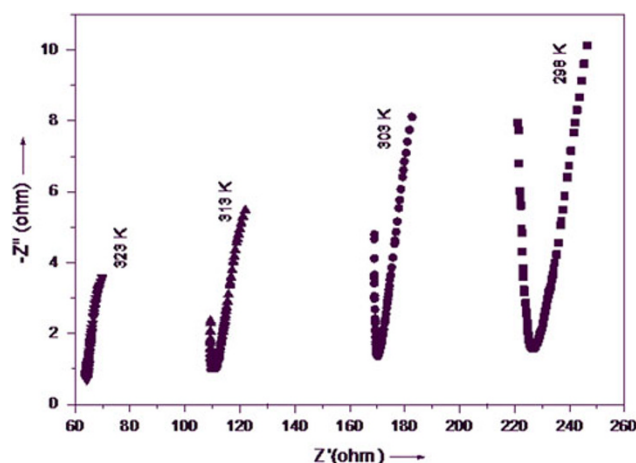


**Fig. 1** Complex impedance plots obtained for the typical composition  $(Ag_4P_2O_7)_{40} - (SbI_3)_{60}$  at 298, 303, 313 and 323 K

**Table 1** Electrical conductivity and ionic transport number results obtained for various compositions of the system  $(\text{Ag}_4\text{P}_2\text{O}_7)_{100-x} - (\text{SbI}_3)_x$ , ( $x = 10, 20, 30, 40, 50, 60, 70, 80$  and  $90$  mol%) at room temperature (298 K)

Composition ( $\times$ mol%)	$\sigma_{298\text{K}}$ ( $\text{S cm}^{-1}$ )	Transport number ( $t_i$ )	
		Wagner's	EMF
$\text{Ag}_4\text{P}_2\text{O}_7$	$2.5 \times 10^{-7}$	–	–
$\text{SbI}_3$ ( $x$ )	$2.2 \times 10^{-6}$	–	–
$x = 10$	$2.3 \times 10^{-7}$	0.76	0.94
$x = 20$	$2.4 \times 10^{-7}$	0.77	0.95
$x = 30$	$1.3 \times 10^{-6}$	0.78	0.94
$x = 40$	$6.7 \times 10^{-6}$	0.83	0.93
$x = 50$	$3.2 \times 10^{-6}$	0.89	0.96
$x = 60$	$4.1 \times 10^{-4}$	0.96	1
$x = 70$	$1.3 \times 10^{-6}$	0.9	0.98
$x = 80$	$2.5 \times 10^{-6}$	0.81	0.98
$x = 90$	$1.4 \times 10^{-7}$	0.63	0.98

temperature dependence of electrical conductivity ( $\sigma$ ) of these materials appears to exhibit Arrhenius-type of behaviour and confirm the presence of crystalline AgI which undergoes  $\beta \rightarrow \alpha$  phase transition at 425 K owing to the appearance of two distinct linear regions below and above 425 K. Though the presence of AgI could be inferred from  $\beta \rightarrow \alpha$  phase transition occurring in the case of those samples having 40, 50 and 70 mol%  $\text{SbI}_3$ , their conductivity values may not be appreciably high, when compared with that of the best conducting composition containing 60 mol%. The difference in such conductivity values may be reasonably interpreted in terms of hard and soft acids and bases (HSAB) criterion. Interestingly, it is clear from Fig. 2 that the series of conductivity plots tend to obey the characteristic Arrhenius relationship below  $t = 425$  K,

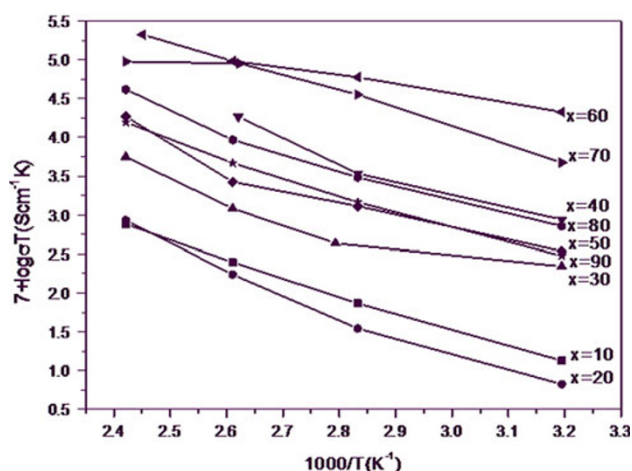


**Fig. 2** Variation of  $\log \sigma T$  as a function of  $1000/T$  for  $(\text{Ag}_4\text{P}_2\text{O}_7)_{100-x} - (\text{SbI}_3)_x$ , ( $x = 10, 20, 30, 40, 50, 60, 70, 80$  and  $90$  mol%) samples

$$\sigma T = \sigma_0 \exp(-E_a/kT) \quad (6)$$

where  $\sigma_0$  is the pre-exponential factor,  $E_a$  the activation energy for conduction,  $k$  the Boltzmann constant and  $T$  is the absolute temperature. As a consequence, the estimated values of  $E_a$  for nine different compositions corresponding to  $x = 10, 20, 30, 40, 50, 60, 70, 80$  and  $90$  mol%  $\text{SbI}_3$  are found to be 0.54, 0.53, 0.59, 0.46, 0.4, 0.2, 0.45, 0.46 and 0.53 eV, respectively. Remarkably, the lowest value of  $E_a$  realized in the case of the best conducting composition containing 60 mol%  $\text{SbI}_3$  may be attributed to the formation of crystalline AgI in this particular specimen dispersed in an amorphous framework as revealed from the present XRD results.

The ion dynamics mechanism in iodide-doped ionic solid materials depends on several factors like the nature of dopant salts, the lattice expansion due to the introduction of the salt, activation energy for ion conduction, mobile ion concentration and the relative environment of the mobile ions (Das et al. 2005). The effect of incorporation of iodide on fast ionic conduction in the case of silver metaphosphate system was earlier studied by (Takahashi et al. 2005) and it was demonstrated that the enhancement in conductivity by the divalent iodide is higher than that in the case of monovalent iodide, whereas the steepest increase in conductivity was obtained only in trivalent iodide-based glasses. Accordingly, it has been concluded that the number of iodide ions is the predominant factor in determining the ionic conductivity in the case of iodide-doped phosphate system (Takahashi et al. 2005). While  $\text{Ag}^+$  ionic conductivity in silver pyrophosphate ( $\text{Ag}_4\text{P}_2\text{O}_7$ ) is found to be of the order of  $10^{-7} \text{ S cm}^{-1}$  at room temperature,  $\text{Sb}^{3+}$  ion is known to bond with non-bridging oxygen in the place of  $\text{Ag}^+$  ion by adding iodide into the system (Kabi and Ghosh 2011). These replaced  $\text{Ag}^+$  ions along with  $\text{I}^-$  ions remain free and cause the expansion of the network. This leads to a more opened up structure suitable for greater  $\text{Ag}^+$  ion conduction. The increase in  $\sigma$  values of these electrolytes could be due to the reaction between the dopant  $\text{SbI}_3$  and  $\text{Ag}_4\text{P}_2\text{O}_7$ , forming AgI during the process of preparation as shown in Fig. 3. AgI may dissociate to provide mobile  $\text{Ag}^+$  ions and thus it may be inferred that mobile  $\text{Ag}^+$  ions are mainly responsible for an increase in the conductivity. Furthermore, as the concentration of trivalent iodide increases above 60 mol%, the conductivity values start decreasing. This could be explained on the basis of the formation of more cross-links in the pyrophosphate network, which makes the structure close-packed and unsuitable for easy migration of  $\text{Ag}^+$  ions (Das et al. 2009). Thus, the mobility of  $\text{Ag}^+$  ions decreases which eventually leads to lower conductivity values.  $\text{Sb}^{3+}$  ion tends to bond with non-bridging oxygen in the place of  $\text{Ag}^+$  ion, by adding antimony iodide into the system, while



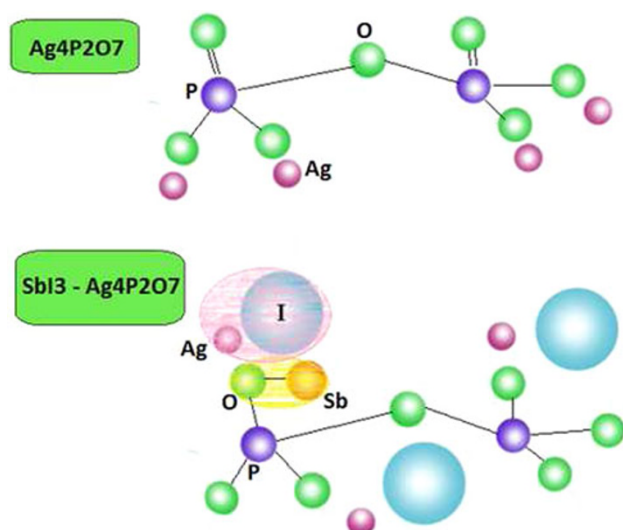


**Fig. 3** Model of AgI ion-pair formation in  $(\text{Ag}_4\text{P}_2\text{O}_7)_{100-x} - (\text{SbI}_3)_x$ , ( $x = 10, 20, 30, 40, 50, 60, 70, 80$  and  $90$  mol%)

some  $\text{Ag}^+$  ions connect with both non-bridging oxygen and iodide ions. The Ag–O bond is considered to be weakened by iodide ions and as a result of this the activation energy decreases and the ionic conductivity increases with increasing  $\text{SbI}_3$  content. The formation of Ag–I pairs is very much essential in order to obtain an appreciably high ionic conductivity for iodide-containing solid electrolytes. The above argument is found to be in conformity with the present XRD and DSC results too.

Figure 4a shows the SEM image of the best conducting composition  $(\text{Ag}_4\text{P}_2\text{O}_7)_{40} - (\text{SbI}_3)_{60}$ , of the present mixed system. The particle size usually plays a vital role on the electrochemical features of device materials. The SEM micrograph of the above sample shows the presence of well defined and densely packed large size crystallites, which are homogeneously distributed without any visible cracks. In addition, at a much higher magnification of 1,50,000 FESEM image, as shown in Fig. 4b, it is clearly confirmed that these particles consist of small crystallites in the nanometer scale and that bigger particles comprised agglomerates of small grains in the micrometer range. The best conducting solid electrolyte material is thus found to contain a mixture of polycrystalline grains with a very wide range of distribution. Interestingly, particle size distribution has been found to be of the order of 9–15 nm and hence such type of morphological features typically encountered under the present experimental conditions is expected to be crucial for electrochemical applications since it develops a high contact surface between the electrolyte and the electroactive material.

The series of room temperature powder XRD patterns obtained for pure specimens of  $\text{Ag}_4\text{P}_2\text{O}_7$ ,  $\text{SbI}_3$  and that of nine different compositions in the mixed system

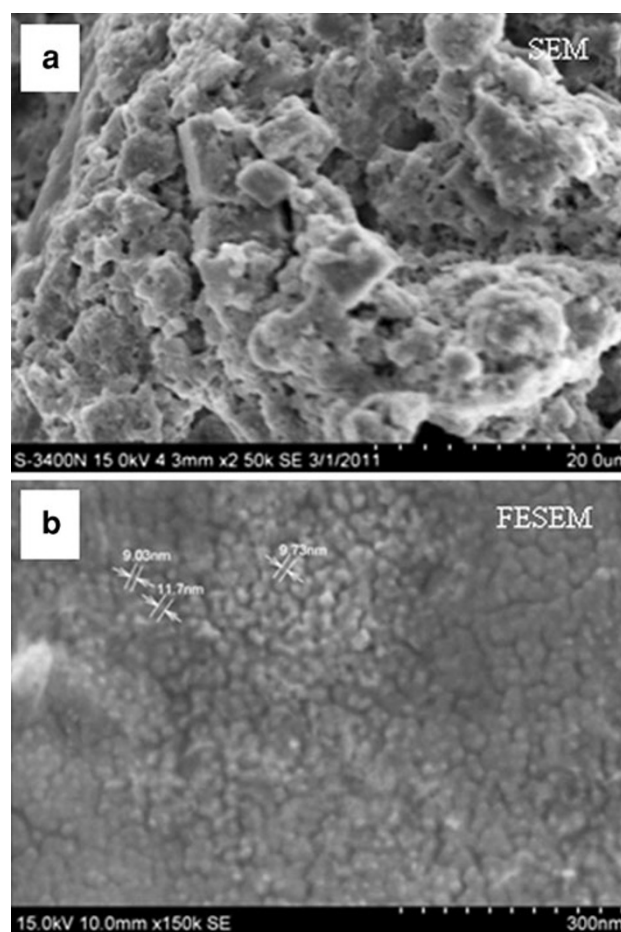


**Fig. 4** a SEM and b FESEM images of  $(\text{Ag}_4\text{P}_2\text{O}_7)_{40} - (\text{SbI}_3)_{60}$  specimen

$(\text{Ag}_4\text{P}_2\text{O}_7)_{100-x} - (\text{SbI}_3)_x$ , ( $10 \leq x \leq 90$ ) are presented in Fig. 5. The detection and identification of reflection lines in all the XRD patterns have been carried out through the XRD analysis software aided by JCPDS-International Centre for Diffraction Data and observed data are presented in Table 2. It is clear from Table 2 and Fig. 5, that the entire series of XRD patterns contain ‘d’ spacings, which are different from that of the starting materials. In the case of a sample having 10 mol%  $\text{SbI}_3$ , XRD peaks noticed at 2.76, 3.02 and 3.3 Å may be attributed to the presence of face-centred orthorhombic phase of  $\text{Ag}_4\text{P}_2\text{O}_7$  (JCPDS file no. 00-040-0058) whereas in the case of a sample having a higher content of 20 mol%  $\text{SbI}_3$ , no sharp peak is observed, and a pair of feeble peaks obtained at 3.43 and 2.55 Å may be due to the formation of certain new intermediate phases. In the case of a composition with 30 mol%  $\text{SbI}_3$ , the single peak appearing at 2.3 Å may be attributed to the presence of  $\text{Ag}_5\text{P}_3\text{O}_{11}$  whereas the sample with 40 mol%  $\text{SbI}_3$  exhibits XRD peaks at 3.74 and 1.94 Å corresponding to AgI. In the case of 30 mol%  $\text{SbI}_3$ ,  $\text{Ag}_3\text{Sb}$  line appearing at 2.82 Å, which may naturally affect the

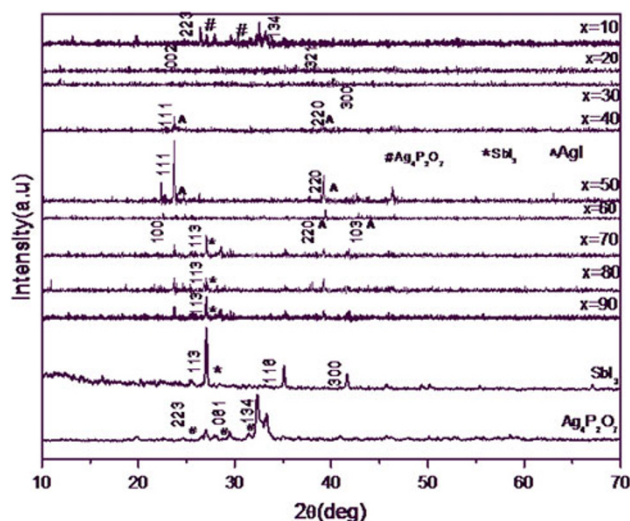


**Fig. 5** Room temperature XRD patterns of  $(\text{Ag}_4\text{P}_2\text{O}_7)_{100-x} - (\text{SbI}_3)_x$ , ( $x = 10, 20, 30, 40, 50, 60, 70, 80$  and  $90$  mol%) samples and that of  $\text{SbI}_3$  and  $\text{Ag}_4\text{P}_2\text{O}_7$

conductivity due to the migration of  $\text{Ag}^+$  ions in AgI. The XRD data corresponding to the composition having 50 mol%  $\text{SbI}_3$  appear to suggest that lines observed at 3.74, 3.96, 2.29 and 1.95 Å could be attributed to the phase  $12\text{AgI} \cdot \text{Ag}_4\text{P}_2\text{O}_7$  (JCPDS file no. 00-033-1186). The XRD result obtained for the best conducting composition in this mixed system, having 60 mol%  $\text{SbI}_3$  appears to show an amorphous background in conjunction with peaks at 3.73, 2.3 and 1.96 Å, which are mainly due to  $\gamma$ -AgI (JCPDS file no. 00-009-0399). In silver iodide, iodide ions are known to form a mixture of closely packed structures at temperatures below 420 K, consisting of fcc and hcp structures which are commonly designated as  $\gamma$ -AgI and  $\beta$ -AgI respectively, whereas those peaks noticed at 2.76, 3.3, 1.57 and 3.03 Å in certain compositions may be assigned to  $\text{Ag}_4\text{P}_2\text{O}_7$ . In the case of compositions containing 70, 80 and 90 mol%, peaks at 3.29, 3.75 and 2.29 Å could be attributed to  $\text{SbI}_3$  in addition to some new additional peaks. From the above discussion, it is therefore clear that all the newly synthesized materials are multiphase in nature consisting of AgI,  $\text{SbPO}_4$ ,  $\text{Ag}_5\text{P}_3\text{O}_{10}$ ,  $\text{Ag}_3\text{Sb}$  and other new phases. These

results are found to be in good agreement with the present DSC data as well. Using the present XRD data, the average crystalline size is also determined using the Scherrer formula

$$D = k\lambda/\beta \cos \theta \quad (7)$$

where  $k$  is a constant taken as 0.9 for calculation,  $\beta$  is full width at half maximum (FWHM) in radian,  $\theta$  the Bragg angle at which the peak maximum occurs and  $\lambda$  is the wavelength of X-ray radiation used. The particle size calculated using the above formula has been found to be consistent with that of FESEM analysis. It is clear from Fig. 5 that the position of typical diffraction peaks corresponding to  $\text{Ag}_4\text{P}_2\text{O}_7$  phase changes successively with the increase of  $\text{SbI}_3$  content. On the other hand, in the case of the compositions containing 20 and 30 mol% of  $\text{SbI}_3$ , a gradual shift in  $d$ -spacing corresponding to  $\gamma$ -AgI, in addition to certain new peaks with a different crystal structure is noticed and this may be due to the possible ion exchange reaction occurring between  $\text{Sb}^{3+}$  and  $\text{Ag}^+$  ions within the material (Padmasree et al. 2005) and the formation of AgI as supported by DSC and conductivity results.

The observed DSC traces in the case of nine different compositions of the mixed system  $(\text{Ag}_4\text{P}_2\text{O}_7)_{100-x} - (\text{SbI}_3)_x$  are shown in Fig. 6. For the purpose of comparison, undoped silver pyrophosphate was also studied. It is evident from Fig. 6 that the characteristic endothermic peaks are observed around 424 K for samples having  $x = 10, 20, 30, 40, 50$  and 60 mol%, respectively. The appearance of such endothermic peaks around 424 K may correspond to the  $\beta \rightarrow \alpha$  transition of AgI, in addition to some other peaks for  $x = 60$  mol% of  $\text{SbI}_3$ . DSC traces recorded for those samples containing less than 50 mol% of  $\text{SbI}_3$  ( $x < 60$ ), are found to indicate a broad exothermic hump typically at 382, 388, 399 and 401 K in the case of samples with  $x = 10, 20, 30$  and 40 mol%, respectively, corresponding to certain characteristic phase transition. On the other hand, the occurrence of two endothermic peaks, one around 425 K and the other around 466 K, in the case of a composition having 50 mol%  $\text{SbI}_3$  has been noticed. The first peak may be attributed to  $\beta$ - $\alpha$  phase transformation of

**Table 2** Observed powder X-ray diffraction (XRD) data for the mixed system  $(\text{Ag}_4\text{P}_2\text{O}_7)_{100-x} - (\text{SbI}_3)_x$  at room temperature

$x = 10$		$x = 20$		$x = 30$		$x = 40$		$x = 50$		$x = 60$		$x = 70$		$x = 80$		$x = 90$	
$d$ (Å)	$I/I^\circ$	$d$ (Å)	$I/I^\circ$	$d$ (Å)	$I/I^\circ$	$d$ (Å)	$I/I^\circ$	$d$ (Å)	$I/I^\circ$	$d$ (Å)	$I/I^\circ$	$d$ (Å)	$I/I^\circ$	$d$ (Å)	$I/I^\circ$	$d$ (Å)	$I/I^\circ$
2.76	100	3.43	40	2.3	35	3.74	100	3.74	100	3.73	100	3.60	100	3.20	100	3.29	100
3.36	74	2.55	19	2.82	27	1.94	37	2.29	85	2.3	84	3.74	20	3.75	18	2.15	50
2.70	65					2.25	30	3.96	60	1.96	45	2.29	34	2.29	29	3.01	45
3.3	62							1.95	50								
3.02	58																
4.48	54																

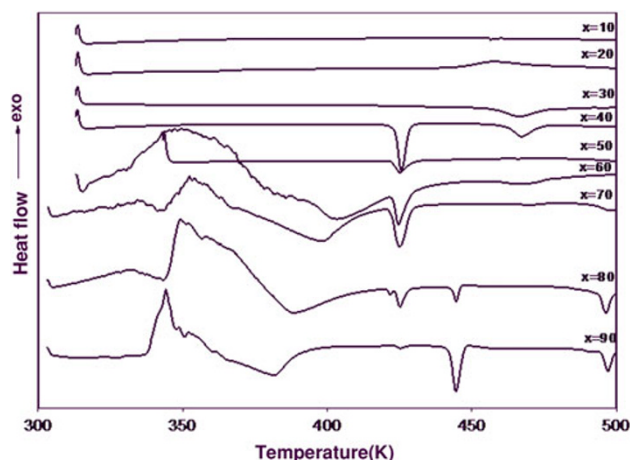
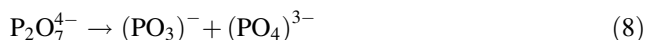


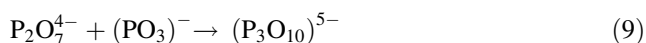
**Fig. 6** DSC traces of  $(\text{Ag}_4\text{P}_2\text{O}_7)_{100-x} - (\text{SbI}_3)_x$ , ( $x = 10, 20, 30, 40, 50, 60, 70, 80$  and  $90$  mol%) samples

AgI (Mroczkowska et al. 2007). The formation of new phase at 466 K may limit the mobility of  $\text{Ag}^+$  ion, thereby reducing the conductivity as expected. Furthermore, the sample having 60 mol% of  $\text{SbI}_3$  shows a very strong endothermic peak at 425 K which clearly confirms the presence of AgI. These endothermic transitions were also found to coincide with corresponding changes observed during the present conductivity measurements. Since the presence of AgI in terms of the  $\beta \rightarrow \alpha$ -phase transition has already been revealed from XRD and conductivity studies as well, the observed endothermic peak around 495 K may be ascribed to the phase transition of unidentified new phases as detected during the XRD analysis.

Figure 7 shows the FTIR absorption spectra observed for all the synthesized compositions of the present system over the wave number range,  $4,000\text{--}400\text{ cm}^{-1}$ . All the prepared samples appear to show absorption bands near  $1,180, 1,040, 950, 725$  and  $520\text{ cm}^{-1}$ , which are assigned to phosphate ion. Pyrophosphate ion is expected to undergo the disproportionation process as proposed by Anantharaj and Rao (1991).



This  $(\text{PO}_3)^-$  ion would act as the primary building unit (a synthon) for further polymerisation.



Hence, a variety of anions could be formed in the case of melt-quenched specimens of solid electrolytes. The typical FTIR spectrum for pyrophosphate consisting of an absorption band near  $1,111\text{ cm}^{-1}$  is assigned to symmetric stretching mode of  $\text{P-O}_i$  bonds of  $\text{PO}_4$  tetrahedra in a chain structure. The next lower frequency mode near  $(1,087\text{--}1,014)\text{ cm}^{-1}$  represents the asymmetric and symmetric vibrations of a  $(\text{PO}_3)^-$  unit that has formed as part of pyrophosphate

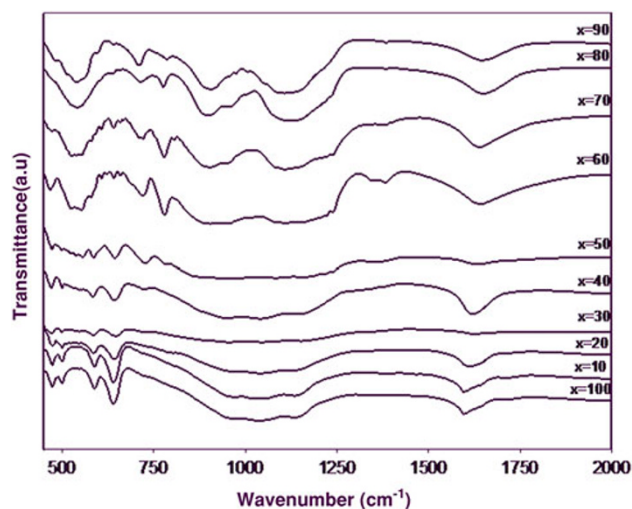


**Fig. 7** FTIR spectra obtained for  $(\text{Ag}_4\text{P}_2\text{O}_7)_{100-x} - (\text{SbI}_3)_x$ , ( $x = 10, 20, 30, 40, 50, 60, 70, 80$  and  $90$  mol%) samples at room temperature

grouping of  $\text{Ag}_4\text{P}_2\text{O}_7$  unit. The asymmetric mode of  $(\text{PO}_3)^-$  unit is strongly excited in IR. Two singlets, centred at  $729$  and  $940\text{ cm}^{-1}$  are attributed to symmetric  $\nu_{1(s)}$  and  $\nu_{2(as)}$  asymmetric P–O–P vibrational modes, respectively and a wide multiplet in the range from  $1,036$  to  $1,254\text{ cm}^{-1}$  corresponds to  $\nu_3$  (P–O) vibration mode. The O–P–O bending vibration  $\nu_4$  is represented by a triplet at  $515\text{--}592\text{ cm}^{-1}$ . Cyclic phosphate is indicated by three bands at  $1,315\text{--}1,255\text{ cm}^{-1}$ . Since no band is present in this region, it is confirmed that no cyclic phosphate is formed. A band around  $870\text{--}900\text{ cm}^{-1}$ , which is the characteristic peak of linear phosphates is observed in the spectra of all the samples investigated and it suggests the presence of linear chain in all the samples prepared. FTIR observations indicate that the band of P–O–P asymmetric stretching mode shifts to higher frequency as the concentration of the dopant increases (Das et al. 2002). The band shift may be explained by the increase in the covalent character of P–O–P bond, which indicates that these bonds are strengthened as more dopant salts are added into the pyrophosphate network and as a result more silver ions could be replaced by the cation M ( $\text{Sb}^{3+}$ ). However, P–O–P bonds in the network are not affected. The formation of P–O–M bonds in the doped system increases the cross-link density in the network.

In order to confirm the results of XRD, DSC and FTIR studies, the transport number of  $\text{Ag}^+$  was also determined by EMF method. Therefore, electrochemical cells having silver anode and iodine cathode were constructed (Padmasree et al. 2005). The ratio between their OCV values and theoretical values gives the transport number ( $t_{\text{Ag}^+}$ ) as  $0.9$ , which indicates that the mobile species involved in the transport process are solely  $\text{Ag}^+$  ions. The fraction of ionic transference number ( $t_i$ ) and conductivity values measured



for all the samples are reported in Table 1. Out of all those synthesized solid electrolytes, the sample having  $x = 60$  mol% exhibited the maximum conductivity within the series and therefore, it is used as the electrolyte for fabricating the solid-state battery. The OCV value of the cell was measured immediately by means of a digital multimeter and found to be 675 mV without any load. The discharge characteristic of the cell was measured at a constant load of 100 k $\Omega$ . For the same load resistance, the voltage  $V$  was measured as a function of time and the discharge time of the cell was found to be nearly 500 h.

## Conclusion

The formation of new superionic solids in the mixed system  $(\text{Ag}_4\text{P}_2\text{O}_7)_{100-x} - (\text{SbI}_3)_x$ , ( $10 \leq x \leq 90$ ) has been investigated by conductivity, ion transport measurements and XRD analysis has revealed the multiphase nature of such superionic solids. DSC results have indicated an endothermic transition occurring at 420 K due to a new phase namely AgI within these materials. FESEM analysis has suggested the presence of nanosized particles within the system and as a consequence, the observed silver ion conductivity has been found to be influenced by the presence of such nanomaterials.

The OCV value of the all solid-state cell prepared with the best conducting solid electrolytic mixture was found to be 675 mV without load. Therefore, this material is found to be one of the most promising candidates for practical applications in the field of solid-state ionics.

**Acknowledgments** The authors are thankful to National Centre for Nanoscience and Technology, University of Madras, for providing necessary facilities for carrying out SEM and FESEM studies. The authors would like to thank SAIF, Indian Institute of Technology, Madras for extending the relevant experimental facility for the present DSC work.

**Open Access** This article is distributed under the terms of the Creative Commons Attribution License which permits any use, distribution, and reproduction in any medium, provided the original author(s) and the source are credited.

## References

- Anantharaj S, Rao KJ (1991) Formation of lead pyrophosphate glass and the role of anion disproportionation. *Proc Indian Acad Sci (Chem Sci)* 103:655–666
- Anantharaj S, Varma KBR, Rao KJ (1986) Thermal properties of silver pyrophosphate-anomalously high glass heat capacities. *Mater Res Bull* 21:1369–1374
- Boukamp BA (1986) A nonlinear least squares fit procedure for analysis of immittance data of electrochemical systems. *Solid State Ionics* 20:31–43
- Das SS, Baranwal BP, Singh P, Srivastava V (2002) Infrared spectroscopic studies of ion-conducting silver phosphate glasses with zinc and cadmium halides. *Prog Cryst Growth Charact Mater* 45:89–96
- Das SS, Gupta CP, Srivastava V (2005) Ion transport studies in zinc/cadmium halide doped silver phosphate glasses. *Ionics* 11: 423–430
- Das SS, Singh NP, Srivastava PK (2009) Ion conducting phosphate glassy materials. *Prog Cryst Growth Charact Mater* 55:47–62
- Das SS, Srivastava PK, Singh NP, Srivastava V (2010) Preparation of some metal chlorides doped silver phosphate glass electrolyte. *Indian J Eng Mater S* 17:123–130
- Dutta D, Ghosh A (2009) Role of  $\text{Ag}_2\text{S}$  nanoparticles on the dynamics of silver ions in silver ultraphosphate glass nanocomposite. *J Phys Chem C* 113:9040–9046
- Kabi S, Ghosh A (2011) Dynamics of  $\text{Ag}^+$  ions and immobile salt effect in  $\text{CdI}_2$  doped silver phosphate glasses. *Solid State Ionics* 187:39–42
- Mroczkowska M, Nowinski JL et al (2007) Micro Raman, FT-IR/PAS, XRD and SEM studies on glassy and partly crystalline silver phosphate ionic conductors. *J Power Sources* 173:729–733
- Murugesan S, Suthanthiraraj SA, Maruthamuthu P (2002) Complex impedance and structural analyses of the mixed system  $40(\text{Cu}_{1-x}\text{Ag}_x\text{I})-30(\text{Ag}_2\text{O})-30(\text{SeO}_2)$ , ( $0.05 \leq x \leq 0.25$ ). *Solid State Ionics* 148:417–423
- Padmasree KP, Kanchan DK, Panchal HR, Awasthi AM, Bharadwaj S (2005) Structural and transport properties of  $\text{CdI}_2$  doped silver ion conducting system. *Solid State Commun* 136:102–107
- Sundar HGK, Liu C, Angell CA (1987) Ionic conductivity in wide range halide-pyrophosphate glasses. *Mater Res Bull* 22:1533–1539
- Takahashi T (1973) Solid silver ion conductors. *J Electrochem* 3: 79–90
- Takahashi H, Nakani H, Sakuma T (2005) Effect of iodide addition on the ionic conduction in silver metaphosphate glasses. *Solid State Ionics* 176:1067–1072